Article

Chelation and nanoparticle delivery of monomeric dopamine to increase plant salt stress resistance

Jiang Du [1,2], Huazhen Xu[1,2], Da-xia Zhang [1] ✉ & Shouqian Feng [1] ✉

Soil salinization hinders sustainable development of global agriculture. Dopamine (DA) delivery is promising for mitigating the detrimental effects of salt on plants. However, self-polymerization limits delivery and effectiveness. Here we chelated DA with ethylenediamine tetraacetic acid and zinc to reduce self-polymerization. To reduce soil adsorption, a sodium lignosulfonate and octadecyl dimethyl benzyl ammonium chloride nanocarrier is made for delivery to the plant. Compared with DA monomer, the soil adsorption rate of the DA in the nanocarrier is 46.02% lower. Salt stress experiments reveal, compared with NaCl and DA groups, the nanocarrier group exhibits significant increases in growth indicators for tomato plants. The beneficial effect is attributed to the increases in proline content, antioxidant capacity, and K$^+$/Na$^+$ ratios in the plants. Similar results are also observed with woody pear seedlings. These findings provide insights into alleviating crop salt stress.

With worldwide agricultural cultivation, the extent and severity of soil salinization have increased annually, posing a significant threat to food security and the environment[1]. The effect of soil salt stress on plant growth is mainly caused by the sodium ions. Elevated concentrations of sodium ions surrounding the root system disrupt the balance of salt ions on the surfaces of the roots, while excessive accumulation of sodium ions within plant tissues perturbs normal metabolic functions, leading to nutrient deficiencies and stunted growth in plants[2,3]. Increased soil quality and higher salt stress tolerance levels of plants have become crucial challenges for ensuring an adequate food supply for an ever-growing population[4].

Due to constraints such as time-consuming procedures, high technological dependency, and unpredictable genetic gains in breeding salt-tolerant varieties[5], researchers have recently shifted their focus towards more easily implemented exogenous growth regulators to increase the salt tolerance of plants, such as brassinolide[6], strigolactone[7], and dopamine (DA)[8,9]. Among them, DA offers the advantages of a lower price, simpler structure, and easier synthetic production. Additionally, the application of exogenous dopamine can enhance photosynthesis under salt stress[9]; increase the activity of antioxidative enzymes to mitigate reactive oxygen species (ROS)

accumulation[10,11]; facilitate the uptake of trace elements while inhibiting the absorption of sodium ions, thereby alleviating salt stress[8]. Furthermore, exogenous dopamine treatment can upregulate the expression of genes associated with salt stress alleviation, thus maintaining a higher K$^+$/Na$^+$ ratio within plants and reducing the damage caused by salt stress[11,12]. However, due to the chemical reactivity of DA, it easily undergoes irreversible self-polymerization reactions to form polydopamine (PDA) during use (Supplementary Fig. 1)[13,14]. PDA is insoluble in water and firmly adheres to solid surfaces such as soil particles and plant roots (Supplementary Fig. 2)[15], thereby significantly reducing the efficiency of DA utilization. Current research in agriculture has focused primarily on utilizing the self-polymerization of DA to confer adhesive functionality and controlled release of carriers[16,17]. At the same time, limited attention has been given to enabling monomer delivery by inhibiting self-polymerization. Florian et al. attempted to delay self-polymerization of DA by adjusting the acidity of the solution, which extended the time for complete self-polymerization from a few minutes to 60 min[18]. Evidently, this extended duration fell short of the duration needed for mitigating plant salt stress, particularly in intricate soil environments where ensuring the stability of DA is even more challenging. Therefore, delaying the self-

[1]Shandong Agricultural University, Tai'an, Shandong, P. R. China. [2]These authors contributed equally: Jiang Du, Huazhen Xu. ✉e-mail: daxia586@163.com; shouqianlove@sdau.edu.cn

polymerization of DA and using it to alleviate plant salt stress has become an urgent issue.

The mechanism of DA self-polymerization is complex and not yet fully understood[19]. Most theories suggest that the catechol groups of DA undergo oxidation to form dopamine-quinone structures, which undergo self-polymerization (Fig. 1a)[20,21]. In this study, a dual-ligand chelation strategy was proposed to delay the self-polymerization of DA through coordination with metal ions (M). However, the findings of this study revealed that the adsorption of DA-metal ion chelates by the soil was prominent, thereby posing persistent challenges for uptake by plants.

Nanotechnology has exhibited remarkable potential in regulating plant growth and alleviating stress[22,23]. The adsorption of nanoparticles in soil has been found to be limited, and their distribution range in soil is extensive[24–26]. The absorption of nanosized metal oxides[27–31] and silicon dioxide[32] by plant roots increase the stress resistance of plants. However, these carriers are unsuitable for this study due to the complex preparation processes, which pose challenges in scaling up production. Moreover, these substances present safety risks to environmental organisms such as zebrafish (*Danio rerio*) and bees (*Apis mellifera Linnaeus*)[33–36]. Therefore, it is urgent to develop nano-delivery systems with simple synthetic processes and excellent bio-compatibilities to apply nanotechnology in the field of plant stress resistance. Currently, there are few reports on the use of nanocarriers for delivering plant growth regulators.

The use of electrostatic self-assembly in constructing lignin-based nanocarrier systems has garnered significant attention. This technology offers advantages such as facile processing and degradable

carriers. Tang et al. employed the electrostatic interaction between sodium lignosulfonate (SL) and cetyltrimethylammonium bromide to fabricate nanoparticles with phenolic hydroxyl, carboxyl and sulfonic acid groups on their surfaces[37], providing abundant binding sites for the adsorption of organic compounds. Nevertheless, the acquisition of the particles required a complex preparation process. Zhang et al. reinforced the carrier by exploiting chelation between the phenolic hydroxyl groups on the lignin carrier surface and Fe^{3+} [38]. Building upon previous research, a one-pot method for constructing lignin-based nanocarriers was developed based on the characteristics of the loaded substances while simultaneously incorporating dual-ligand dopamine without the need for ultrasonication, centrifugation, and drying processes.

In this study, we chelated DA with ethylenediamine tetraacetic acid (EDTA) and zinc to form the dual-ligand chelated EDTA/Zn/DA (EZD), thereby reducing self-polymerization. Subsequently, electrostatic self-assembly is employed in construction of a lignin-based nanocarrier system loaded with EZD to mitigate soil adsorption of the organic compounds. The underlying mechanism behind the formation of this delivery system is revealed. This delivery system comprises EDTA, zinc, SL, and octadecyl dimethyl benzyl ammonium chloride (ODBAC). Despite the complexity of its components, the system is composed of low-cost chemical products. Furthermore, the system can be synthesized successfully at room temperature and pressure within a short timeframe. By assessing the ability of dopamine and its derivatives to alleviate salt stress in tomato and pear seedlings and examining the spatial distributions of Na$^+$ and K$^+$ within the plant tissues, the mechanism by which DA alleviates salt stress is elucidated. These findings offer a promising avenue for practical utilization of DA while offering technical support and a theoretical foundation for managing crop salt stress.

## Results and discussion
Construction of EZD

Coordination of Zn^{2+}, Fe^{2+}, and Fe^{3+} with DA was investigated with molar ratios of M:DA = 1:2 based on chelation of the metal ions (M) with phenolic hydroxyl groups to inhibit dopamine self-polymerization. Immediate formation of black–green precipitates was observed for Fe^{2+} and Fe^{3+} upon coordination with DA (Supplementary Fig. 3a, b); Zn^{2+} significantly delayed the self-polymerization of DA; however, a brown–yellow aggregate also appeared in the Zn/DA solution after 24 h (Supplementary Fig. 3c).

EDTA is commonly employed as a metal ion chelator in trace element fertilizers[39]. In this study, EDTA was incorporated into the Zn/DA system to inhibit the self-polymerization of DA by increasing the molecular weight of the compound and introducing steric hindrance (Fig. 1b). Preliminary experiments demonstrated a noteworthy reduction in self-polymerization when the EZD ratio was adjusted to 1:1:2 (Supplementary Fig. 3d). Subsequently, the proportions of the individual components in EZD were further optimized.

Due to the self-polymerization of the Zn/DA, the EDTA/Zn ligand was initially prepared to ensure the absence of free Zn^{2+} within the system. The ultraviolet–visible (UV–Vis) spectra were measured for various ratios of EDTA/Zn in the solutions with an UV–Vis spectro-photometer. As shown in Fig. 2a, the absorbance of EDTA/Zn was significantly greater than that of EDTA. The maximum absorption wavelength was redshifted from 280 nm to 285 nm after EDTA chelation of Zn^{2+}, consistent with previous findings of Zhao et al. regarding a redshift in the maximum absorption wavelength after Au^{3+} was chelated with EDTA[40]. Within the range of 1:0.5–1:1 ratios for EDTA and Zn, as the proportion of Zn^{2+} increased, the absorbance of the EDTA/Zn solution gradually increased. Therefore, within this range, all of the Zn^{2+} in solution was coordinated by EDTA. Based on this observation, two ratios (EDTA/Zn = 1:0.5 and 1:0.8) exhibiting significantly different absorbances were selected for investigating DA chelation.
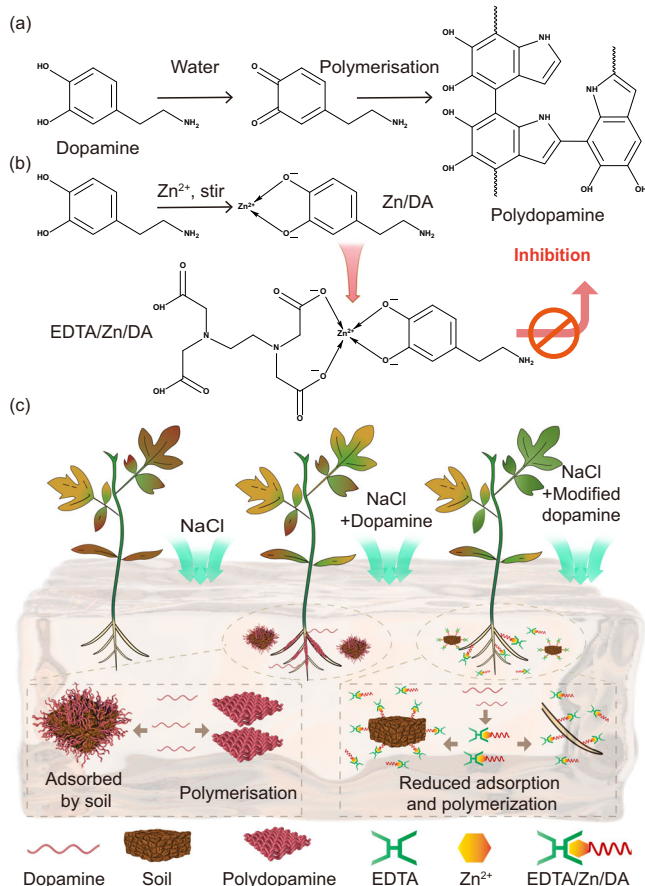
Fig. 1 | Schematic diagram of EZD synthesis and its inhibition of dopamine self-polymerization to enhance dopamine bioavailability. a Potential mechanism for dopamine polymerization; **b** binding mode of EDTA, Zn^{2+}, and DA; **c** Schematic showing how EZD reduced soil adsorption and alleviated plant salt stress.
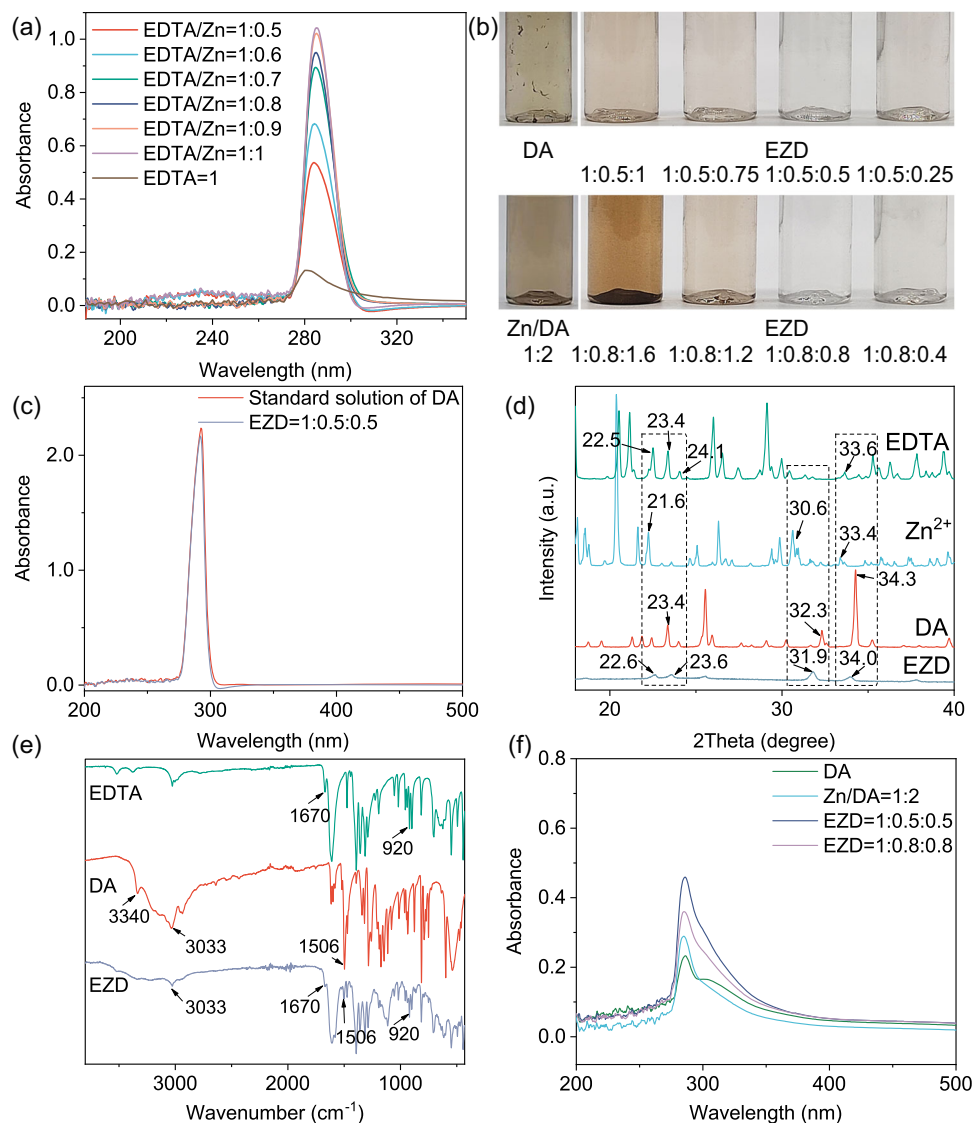
Fig. 2 | Characterization of EZD. a UV–Vis spectra of EDTA/Zn; **b** appearance of samples containing dopamine after 30 days; **c** UV–Vis spectra of EZD; **d** XRD spectra, and **e** FTIR spectra of EZD; **f** UV–Vis spectra of four dopamine samples adsorbed by soil.

An EDTA/Zn deionized aqueous solution was mixed with various concentrations of deionized aqueous DA solutions to obtain dual-ligand EZD ratios of 1:0.5:0.25, 1:0.5:0.5, 1:0.5:0.75, 1:0.5:1, 1:0.8:0.4, 1:0.8:0.8, 1:0.8:1.2, and 1:0.8:1.6. As shown in Fig. 2b, significant self-polymerization occurred in the DA and Zn/DA deionized water solutions after they stood for 2 days. However, no apparent self-polymerization was observed for the four EZD solutions with ratios of 1:0.5:0.25, 1:0.5:0.5, 1:0.8:0.4, and 1:0.8:0.8 after they were left at room temperature for 30 days. UV–Vis spectroscopy showed that the absorption spectra of EZD (ratio of 1:0.5:0.5) were consistent with those of the DA solutions, indicating that no chemical structural changes occurred during chelation of EDTA/Zn with DA (Fig. 2c).

During the application process, it is essential to dilute the solution with tap water; therefore, an investigation was conducted to assess the stabilities for various proportions of EZD diluted solutions. The above 10 samples were diluted with tap water to give DA concentrations of 50 µmol L^{-1}. After 6 h, aggregation was observed in both the DA and Zn/DA diluted solutions, while the EZD diluted solution remained stable. Even after 96 h, no apparent aggregation was observed in the EZD solutions with ratios of 1:0.5:0.25, 1:0.5:0.5, 1:0.8:0.4, and 1:0.8:0.8 (Supplementary Fig. 4).

In conclusion, the proposed dual-ligand scheme mitigated the self-polymerization of DA. Two samples (1:0.5:0.5 and 1:0.8:0.8) with relatively high proportions of the chelating DA were selected for subsequent research.

Characterization of EZD

The crystal structure of EZD was determined by X-ray diffraction (XRD) analysis. As shown in Fig. 2d, the diffraction peak for EZD at 34° was almost identical to that for DA at 34.3°. After synthesis of the dual ligand complex, a new diffraction peak for EZD appeared at 31.9°, positioned between the peaks corresponding to Zn^{2+} at 30.6° and DA at 32.3°. The diffraction peak for EZD at 22.6° was nearly identical to that for EDTA at 22.5°, and the peak at 23.6° was almost the same as those for EDTA and DA at 23.4°. Moreover, the diffraction peak intensities of the dual-ligands were significantly less than those of the three monomers, indicating lower crystallinity of EZD. These results provided evidence for the formation of EZD.

Fourier-transform infrared (FTIR) spectroscopy is commonly employed to identify changes in functional groups within compounds and reveal reaction mechanisms. The FTIR spectra of EDTA, DA, and EZD are shown in Fig. 2e. For EDTA, the peak at 1670 cm^{-1} was attributed to stretching vibrations of the C = O bonds, while the peak at

920 cm^{-1} corresponded to the O-H bending vibrations of COOH groups. These peaks were also present in the spectrum of EZD, indicating the presence of EDTA within EZD. Additionally, a decrease in the intensity of the OH absorption peak suggested that OH provided a binding site for Zn^{2+} to form the coordination bond with EDTA. In the DA spectrum, the stretching vibrational peak at 3340 cm^{-1} corresponded to the phenolic hydroxyl group, while the peaks at 3033 cm^{-1} and 1506 cm^{-1} corresponded to the N-H stretching vibrations and skeletal vibrations of the benzene ring, respectively. The peaks of the phenolic hydroxyl group and benzene ring appeared in the EZD spectrum with significantly reduced intensities, indicating that the phenolic hydroxyl group functioned as a binding site for Zn^{2+} and formed coordination bonds with DA. Therefore, the mechanism for formation of the dual-ligand EZD involved coordination of Zn^{2+} with the hydroxyl groups on both EDTA and DA.

To ensure the efficacy of applying the DA in soil, soil adsorption tests were conducted to evaluate absorption of the dual-ligands by plants. As shown in Fig. 2f, the rates for adsorption of DA and Zn/DA by soil were 75.89% and 70.06%, respectively, when compared with the absorbance values for a standard solution containing 4 mmol L^{-1} DA (Supplementary Fig. 5). Notably, the EZD = 1:0.5:0.5 and 1:0.8:0.8 groups exhibited significant improvements, and the adsorption rates were decreased to 52.41% and 62.73%, respectively. It was inferred that soil adsorption significantly reduced the utilization efficiency of DA; although dual-ligands had proven effective in mitigating soil adsorption, there was still room for further enhancement.

In recent years, nanotechnology has demonstrated significant potential in limiting the adsorption of organic matter by soil[41,42]. This study was intended to increase the efficiency of dopamine utilization in soil through nanotechnology by selecting EZD = 1:0.5:0.5 with lower rates of soil adsorption for subsequent research.

Construction of lignin-based nanodelivery system

Initially, this study aimed to employ an environmentally friendly SL to adsorb EZD and enable one-step preparation of nanoparticles. However, the two substances did not form stable particle structures in aqueous solutions; instead, they formed flocculent precipitates (Supplementary Fig. 6). UV–Vis analyses revealed spectra for the flocculent precipitates that differed from those of SL and EZD (Supplementary Fig. 7). Although the desired nanoparticles were not obtained, strong adsorption of SL and EZD was observed. This has valuable implications for nanoparticle syntheses.

At this stage, our research focus shifted to the construction of nanoparticles containing SL on the surface for loading the EZD. Some lignin-based nanoparticles are manufactured through electrostatic interactions between SL and quaternary ammonium salts, involving a centrifugation cleaning step[43]. The aim of this study was to establish a simpler and milder one-pot method for synthesizing nanoparticles, thereby facilitating future large-scale applications. To mitigate the aggregation observed when directly mixing the oil phase containing the quaternary ammonium salt with the SL water phase (Supplementary Fig. 8), the following process was established. First, an oil-in-water emulsion of ODBAC was prepared and subsequently introduced into the aqueous SL solution (Fig. 3a). As a result, particle aggregation was significantly reduced (Supplementary Fig. 9), enabling the successful synthesis of lignin-based nanocarriers (ODBAC/SL). Finally, ODBAC/SL was added to the EZD solution to obtain the nanoparticles (ODBAC/SL-EZD).

Characterization of ODBAC/SL-EZD

The formation of nanoparticles mainly involves electrostatic attractions between substances with opposite charges; therefore, the reaction was initially assessed by monitoring the *zeta* potential. As shown in Fig. 3b, ODBAC contains N$^+$, and the emulsion exhibited a *zeta* potential of 59.37 mV. The *zeta* potential of ODBAC/SL was −28.20 mV,

indicating that SL was adsorbed by ODBAC and deposited onto the surfaces of the emulsion droplets, resulting in negatively charged particles. After EZD (1:0.5:0.5) adsorption, the electronegativity of ODBAC/SL-EZD decreased to −16.34 mV and decreased further with increasing EZD content. Therefore, the adsorption phenomenon between ODBAC/SL and EZD were related to their charged functional groups.

The crystal structure of ODBAC/SL-EZD was determined through XRD analysis. As shown in Fig. 3c, ODBAC exhibited high crystallinity, while SL displayed an amorphous structure. The spectrum of ODBAC/SL-EZD was intermediate between those of ODBAC and SL, characterized by a broader peak and an amorphous substance. Notably, the intensity of the bread peak at 10–30° for ODBAC/SL-EZD surpassed that observed for ODBAC/SL.

The average particle sizes of ODBAC/SL and ODBAC/SL-EZD were 195.14 ± 2.53 and 199.98 ± 5.58 nm, respectively (Fig. 3d). The smaller ODBAC/SL particles experienced rupture and aggregation during the drying process, whereas the adsorption of EZD significantly reinforced ODBAC/SL, enabling the 50 nm particles to maintain spherical shapes (Fig. 3e, f). Additionally, thermogravimetric analyses indicated that the degradation of ODBAC/SL was significantly faster than that of ODBAC/SL-EZD (Supplementary Fig. 10). These results demonstrated the crucial role of EZD in reinforcing the nanoparticles and confirmed its presence within them.

## Formation mechanism for ODBAC/SL-EZD

FTIR spectroscopy was employed to reveal the chemical structure changes occurring during formation of the nanoparticles. The spectra of ODBAC, SL, ODBAC/SL and ODBAC/SL-EZD were shown in Fig. 4a. For ODBAC, the peaks at 2920 and 2850 cm^{-1} were attributed to the stretching vibrations of methyl and methylene groups, and they were also present in the spectra of ODBAC/SL and ODBAC/SL-EZD; the peak at 1640 cm^{-1} for ODBAC was attributed to C-N stretching vibrations. For SL, the peak at 3500–3200 cm^{-1} was attributed to stretching vibrations of phenolic hydroxyl groups, the peak at 1590 cm^{-1} was assigned to the antisymmetric stretching vibration of COOH, and the peaks at 1130 and 1030 cm^{-1} corresponded to the stretching vibrations of SO$_3^-$. After electrostatic self-assembly of ODBAC and SL, the peak intensities for C-N, phenolic hydroxyl groups and COOH decreased significantly, while there was little change in the intensity of the SO$_3^-$ peak. Combined with the *zeta* potentials, these results indicated that electrostatic interactions occurred among N$^+$, ionized COO$^-$ and phenolic hydroxyl groups, which was consistent with previous research[44].

In the ODBAC/SL-EZD spectra determined after adsorption of EZD onto ODBAC/SL, the benzene ring vibration peak of DA appeared at 1506 cm^{-1} in the ODBAC/SL-EZD spectrum. Additionally, decreased intensity was observed for the N-H peak at 3033 cm^{-1} in the EZD spectrum and the peak at 1030 cm^{-1} for SO$_3^-$ in ODBAC/SL within the ODBAC/SL-EZD spectrum, indicating that electrostatic interactions between N-H and SO$_3^-$ facilitated EZD deposition on the nanoparticles.

The surface elements of the nanoparticles were determined with X-ray photoelectron spectroscopy (XPS). Adsorption of the EZD onto ODBAC/SL led to significant increases in the intensities of the O 1s, N 1s, and C 1s peaks, while minimal changes in the S 2p peak were observed (Fig. 4b). As shown in Fig. 4c, a comparison of the absorption peaks for the key element (Zn) in the two samples revealed the absence of a Zn absorption peak for ODBAC/SL. The peaks at 1044.8 and 1021.8 eV in the ODBAC/SL-EZD spectrum correspond to the Zn 2$p_{1/2}$ and Zn 2$p_{3/2}$ binding energies, respectively.

Based on the above results, a mechanism for the formation of nano-ODBAC/SL-EZD (Fig. 4e) was developed. The ODBAC emulsion was positively charged due to N$^+$, while the weakly alkaline SL solution underwent ionization of the sulfonic groups, carboxyl groups, and
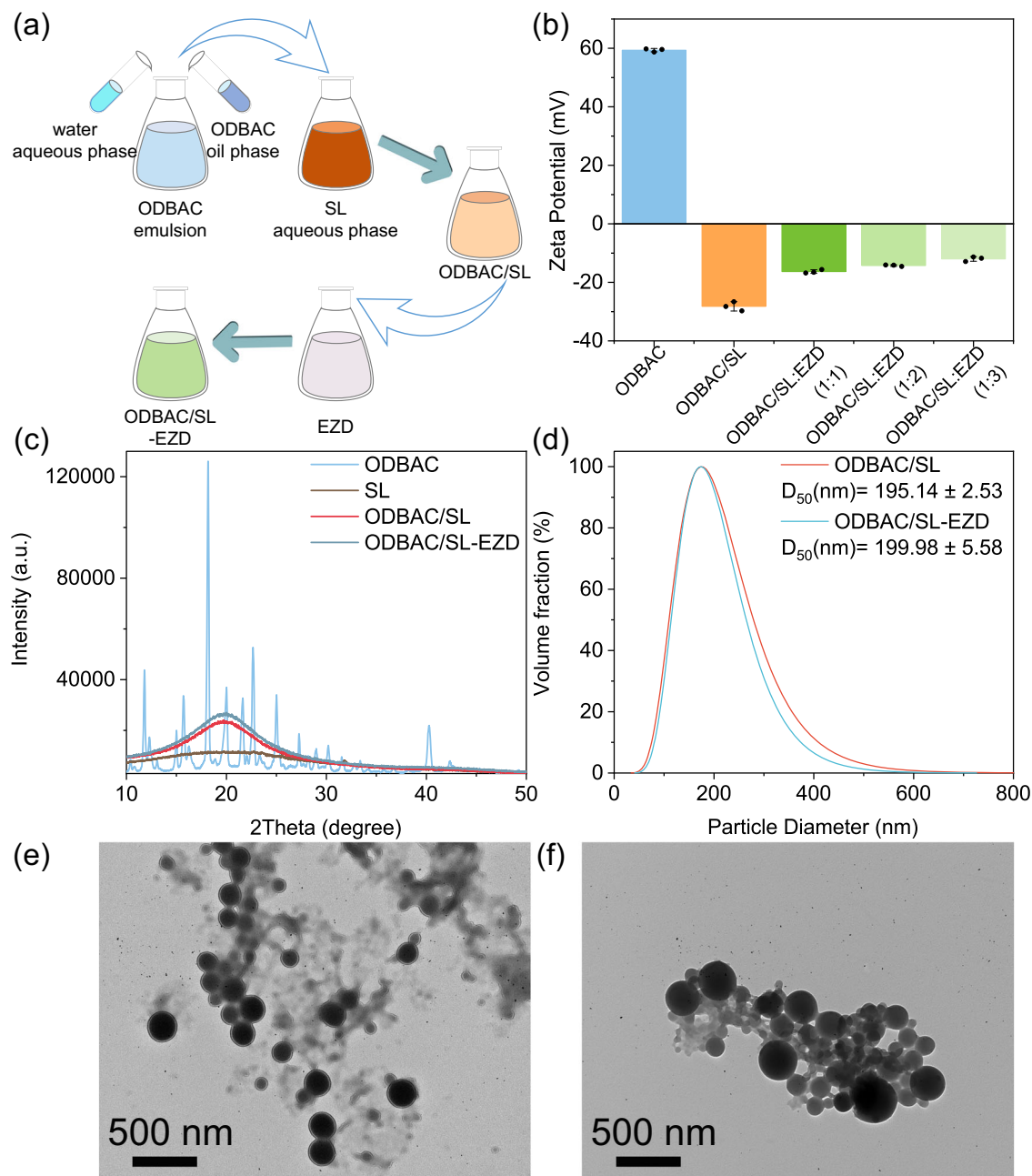
Fig. 3 | Characterization of ODBAC/SL-EZD. a Schematic showing fabrication of the ODBAC/SL and ODBAC/SL-EZD; **b** *Zeta* potential changes during the formation of nanoparticles (*n* = 3 independent experiments, the data are presented as means ± SD); **c** XRD spectra of ODBAC/SL and ODBAC/SL-EZD; **d** Particle size distributions of ODBAC/SL and ODBAC/SL-EZD; Transmission electron microscopy (TEM) images of (**e**) ODBAC/SL and (**f**) ODBAC/SL-EZD.

phenolic hydroxyl groups, resulting in negatively charged SL[45,46]. The negatively charged groups established electrostatic interactions with N+, resulting in the complexation of SL and ODBAC and the formation of negatively charged ODBAC/SL nanoparticles. After the addition of EZD, electrostatic interactions between the N-Hs of EZD and the SO_3^- on the surface of ODBAC/SL occurred, ultimately forming ODBAC/SL-EZD.

Soil adsorption of ODBAC/SL-EZD
To assess the efficacy of using nanotechnology to reduce the adsorption of dopamine by soil, an additional soil adsorption experiment was conducted. As shown in Fig. 4d, the adsorption extent of DA on ODBAC/SL-EZD was significantly lower than those of the EZD samples, with only 29.87% of the DA adsorbed. This was 46.02% lower than the

adsorption rate of monomeric DA and 22.54% and 32.86% lower than the adsorption rates of EZD = 1:0.5:0.5 and 1:0.8:0.8, respectively. These results demonstrated the feasibility of employing the nanotechnology developed in this investigation to increase DA utilization.

Distribution of nanoparticles in plant roots
The root uptake of ODBAC/SL-EZD plays a pivotal role in the efficacy of dopamine, so the distributions of ODBAC/SL and ODBAC/SL-EZD within roots were evaluated. Fluorescence tracing revealed that nanoparticles were distributed in the root epidermis (Fig. 5c, e) and penetrated the epidermis to the endodermis and xylem cells of the root (Fig. 5d, f). This was consistent with previous research showing that nanoparticles penetrated the epidermis of tomato roots to reach the interior[47,48].
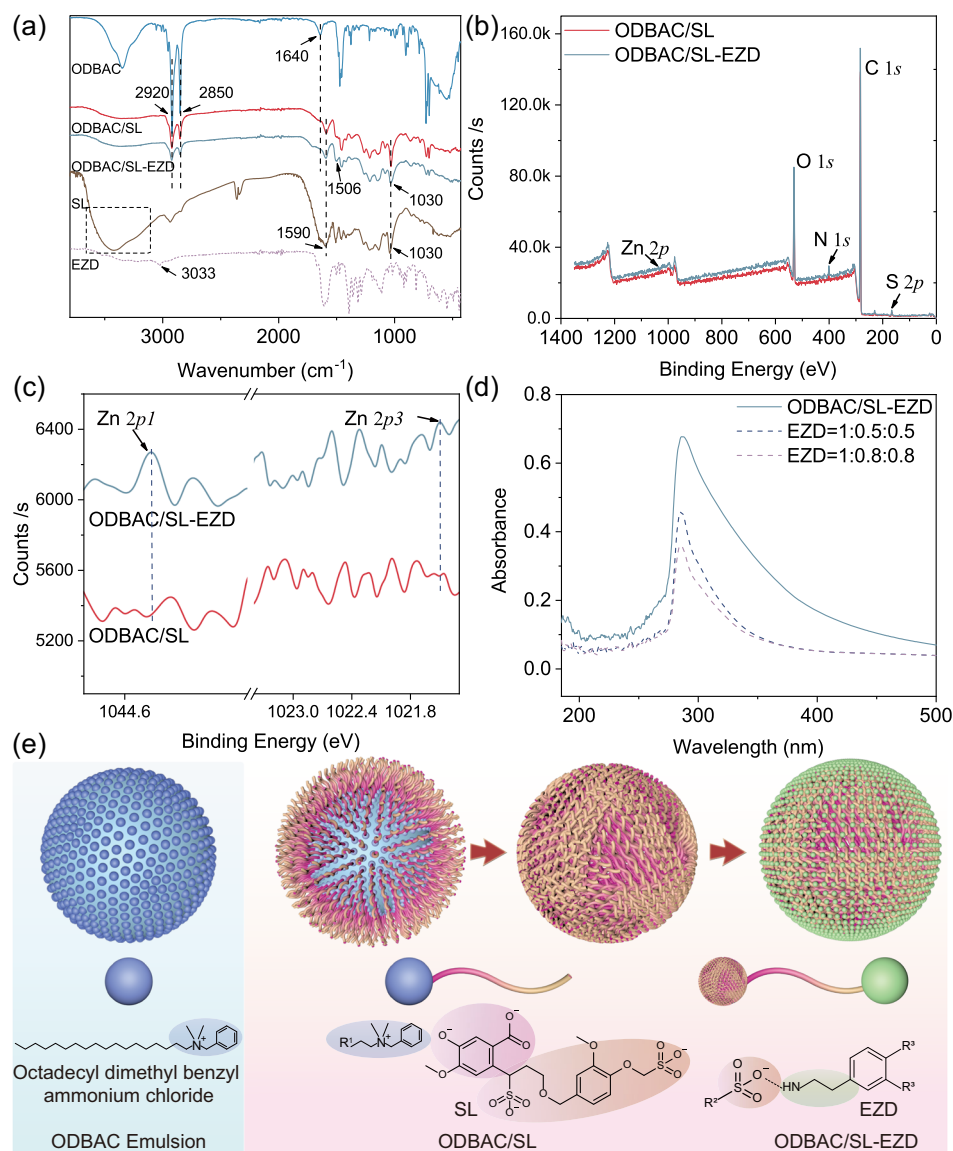
Fig. 4 | Formation mechanism for ODBAC/SL-EZD. a FTIR spectra for the nanoparticles; **b, c** XPS spectra of ODBAC/SL and ODBAC/SL-EZD; **d** UV–Vis absorbance spectra of ODBAC/SL-EZD adsorbed by soil; **e** Schematic showing the formation mechanism for ODBAC/SL and ODBAC/SL-EZD.

Loading rate of the DA

The titration method was employed to determine the loading rate of DA in ODBAC/SL-EZD, as DA forms purple–red complexes with $FeCl_3$ in ammonia solutions. The results showed that the loading rate of DA was $21.40 \pm 1.14\%$.

Amelioration of salt-induced phenotypic deterioration in tomato and pear seedlings with ODBAC/SL-EZD

To validate the alleviation effects of different treatments, it was first evaluated whether EZ and blank ODBAC/SL nanoparticles alone can alleviate plant salt stress. The tomato and pear seedlings were treated with EZ and blank ODBAC/SL nanoparticles, followed by salt stress application. The results indicated that tomato seedlings treated with EZ or ODBAC/SL nanoparticles exhibited pronounced salt stress symptoms after salt treatment (Supplementary Fig. 11a), such as leaf wilting and yellowing, substantial reductions in plant heights, root elongations, root tips number, and root surface areas, along with significant increases in proline, superoxide anion (O_2^-), and malondialdehyde (MDA) contents in leaves (Supplementary Fig. 11b–i), compared with untreated controls. Moreover, no significant differences were observed between these treatments and the salt stress-only

group. This indicated that EZ or ODBAC/SL nanoparticles alone were not effective in alleviating salt stress in tomato plants. Similar results were obtained in pear seedlings under the same experimental conditions (Supplementary Fig. 12). Consequently, this experiment did not demonstrate that the carrier materials possessed the capability to alleviate plant salt stress.

The comparative efficacies of PDA, DA, Zn/DA (1:2), EZD (1:0.5:0.5), and ODBAC/SL-EZD in attenuating salt-induced phenotypic damage to tomato and pear seedlings were further evaluated. After a 20-cycle sodium chloride exposure regimen, the tomato seedlings exhibited pronounced salt stress phenotypes (Fig. 6b), including a significant reduction in chlorophyll content in the upper foliage and marked decreases in the plant stature, root elongation, root tip proliferation, and root surface area expansion (Fig. 6h–l and Supplementary Fig. 13). Key physiological indicators of salt stress, including proline, O_2^-, and MDA levels, were significantly elevated (Fig. 6m–o). In contrast to the saline control, PDA application did not alleviate these salt-induced defects (Fig. 6c). Although the DA and Zn/DA treatments preserved some growth attributes under saline conditions, the foliage displayed evident stress markers (Fig. 6d, e). Conversely, the EZD and ODBAC/SL-EZD treatments notably diminished the detrimental effects
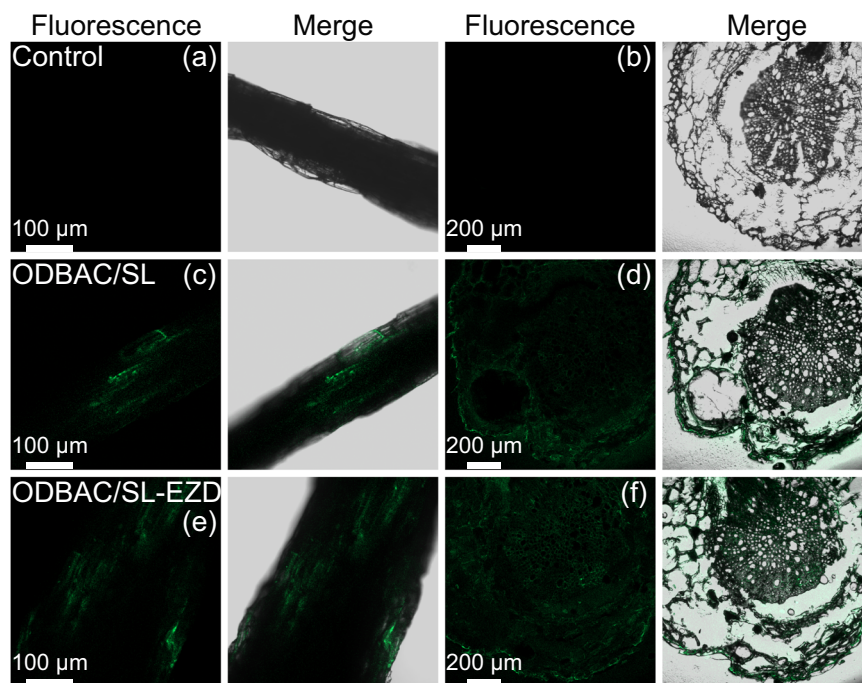
Fig. 5 | Distribution of nanoparticles within the plant roots. a Surface and **b** cross-sections of roots from the control group; **c, e** surface and **d, f** cross-sections of roots treated with ODBAC/SL and ODBAC/SL-EZD. Each experiment was repeated three times independently with similar results.

of salt stress, with the latter conferring the most pronounced benefits (Fig. 6f, g). Seedlings treated with ODBAC/SL-EZD retained the verdant upper leaves (Fig. 6g) and exhibited substantial enhancements in vegetative growth parameters. Proline content was elevated, while the levels of O_2^- and MDA were significantly suppressed. These outcomes surpassed those observed in the saline control and other treatment groups (Fig. 6h–o). Analogous outcomes were discerned for pear seedlings challenged with salt stress, where ODBAC/SL-EZD significantly eclipsed alternative treatments in stress mitigation (Supplementary Figs. 14–17).

Under salt stress, plants accumulate proline to maintain osmotic balance. However, salt stress also leads to a significant increase in ROS, such as O_2^-, and MDA, causing cellular membrane damage and a subsequent decline in chlorophyll content, which inhibits photosynthesis. Previous research has indicated that DA administration can alleviate salt stress in fruit trees[10]. Nonetheless, the propensity of DA for soil particle adsorption and spontaneous polymerization into PDA reduce its therapeutic potential and increase the deployment costs. To address these limitations, a strategy was developed that integrated dual-ligand chelation with nanoparticle adsorption to increase the stability and soil-binding resistance of the active agent. This approach enabled ODBAC/SL-EZD to inhibit DA autopolymerization and enhance its soil adsorption resilience. Furthermore, ODBAC/SL-EZD treatment promotes proline accumulation, scavenges ROS, and protects chlorophyll in tomato plants, effectively mitigating the detrimental effects of salt stress on plant growth and significantly improving salt tolerance. This refined formulation demonstrates a greatly enhanced capacity for DA to alleviate plant salt stress.

ODBAC/SL-EZD facilitates K^+/Na^+ homeostasis, mitigating salt stress in tomato and pear seedlings
Plant salinity tolerance is critically dependent on the ability to mitigate intracellular Na^+ accumulation and promote vigorous K^+ uptake under high salinity conditions, which necessitates the preservation of a high K^+/Na^+ ratio for cellular integrity and growth of salt-tolerant plants[11,49,50]. This investigation quantified the K^+ and Na^+ concentrations in the leaves, stems and roots tissues of tomato and pear plants

treated with PDA, DA, Zn/DA, EZD (1:0.5:0.5), or ODBAC/SL-EZD under saline conditions. The calculations of the tissue-specific K^+/Na^+ ratios were based on these ionic contents. The results revealed that ODBAC/SL-EZD treatment markedly reduced the tissue-specific K^+ and Na^+ levels (Fig. 7a, c, e) and increased the K^+/Na^+ ratios in the roots, stems, and leaves of both tomato and pear plants (Fig. 7b, d, f and Supplementary Fig. 18).

To further investigate the specific mechanisms by which nano-sized dopamine enhances plant salt tolerance, the expression levels of genes associated to Na^+/K^+ transport were analyzed. Under salt stress, plants activate the salt overly sensitive (SOS) pathway and the Na^+/H^+ antiporter SOS1 to expel Na^+ from the cytoplasm to the extracellular space, reducing cytotoxic effects[51]. The high-affinity K^+ transporter (HKT1) is crucial for salt tolerance as it minimizes Na^+ accumulation in shoots and retrieves it from xylem sap, regulating its distribution between roots and shoots[52,53]. HKT1 collaborates with the SOS pathway to indirectly contribute to Na^+/K^+ homeostasis[54]. Moreover, vacuolar Na^+ sequestration, facilitated by the Na^+/H^+ exchanger (NHX1), aids in mitigating ionic toxicity within the cytosol[55,56]. Collectively, these processes improve plant resilience to salt stress by increasing the cellular K^+/Na^+ ratio. Consequently, this study measured the relative expression levels of *SlHKT1;2*, *SlNHX1*, and *SlSOS1* in the leaves and roots of tomato plants treated with PDA, DA, Zn/DA, EZD (1:0.5:0.5), or ODBAC/SL-EZD under saline conditions. The results indicated that ODBAC/SL-EZD treatment significantly upregulated the expression levels of *SlHKT1;2*, *SlNHX1*, and *SlSOS1* in tomato leaves, stems and roots (Fig. 8). Furthermore, control experiments revealed that the application of EZ or the empty ODBAC/SL nanocarrier alone had no effect on the expression of these three genes in the leaves, stems, or roots under salt stress (Supplementary Fig. 19). This indicates that ODBAC/SL-EZD can effectively enhance the expression of ion transport-related genes, contributing to the maintenance of ion homeostasis in plants under salt stress conditions.

The contribution of dopamine to alleviation of the salt stress in plants predominantly involved the regulation of K^+ and Na^+ levels. On the one hand, dopamine stimulates the expression of *SOS1*, facilitating
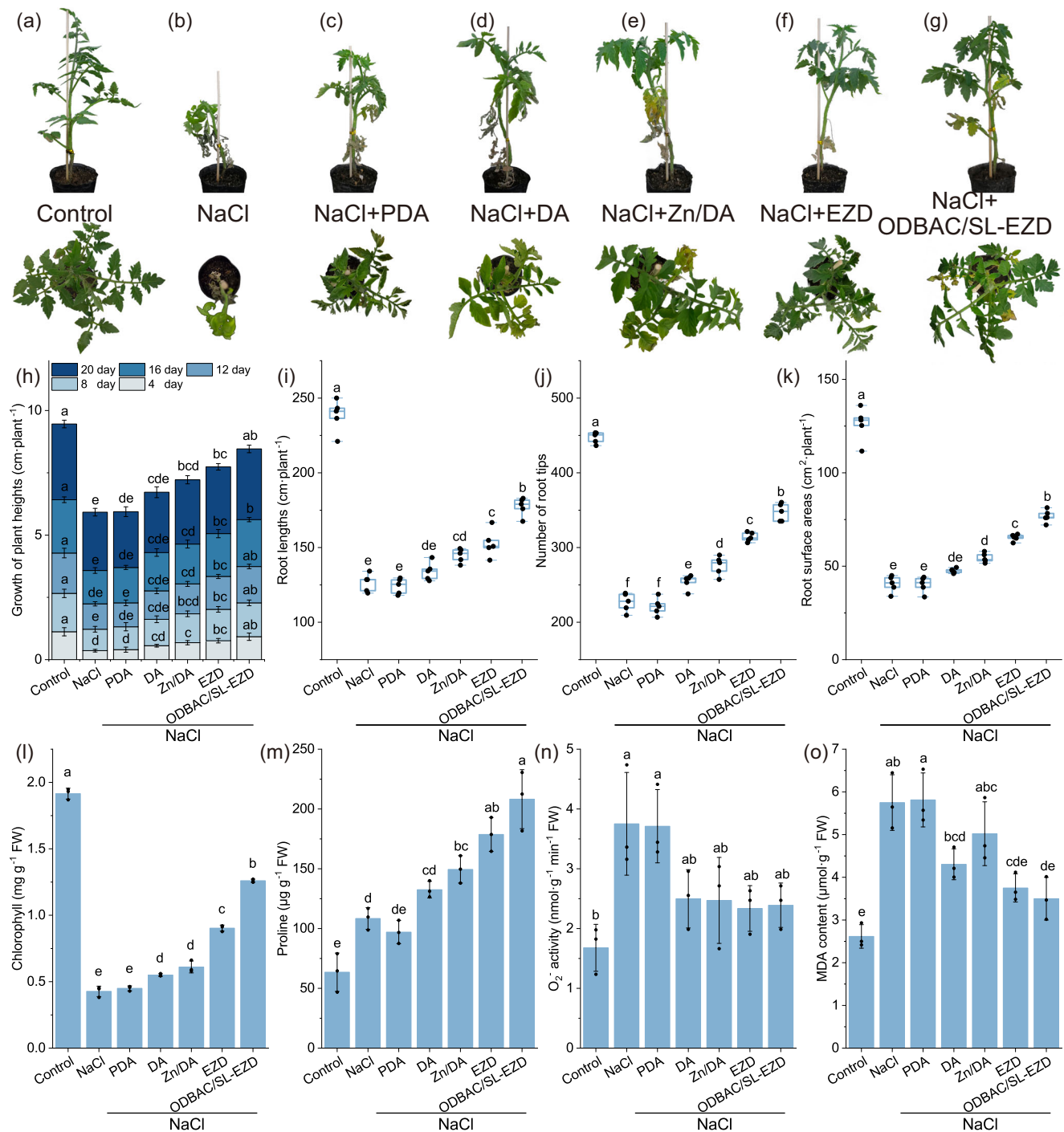
Fig. 6 | Effects of dopamine and its derivatives on physiological and biochemical indices of NaCl-stressed tomato seedlings. Images of tomato plants treated with **a** control, **b** NaCl, **c** NaCl+PDA, **d** NaCl+DA, **e** NaCl+Zn/DA, **f** NaCl+EZD, and **g** NaCl+ODBAC/SL-EZD after 20 treatment cycles; **h** growth of plant heights ($n = 5$ independent experiments, bars represent the means ± SD), **i** root lengths, **j** number of root tips, and **k** root surface areas ($n = 5$ independent experiments, individual data point represents the means. Boxes represent the 25th–75th percentile range, white lines represent medians and whiskers show the minimum-maximum range); **l** chlorophyll content, **m** proline, **n** O_2^- activity, and **o** MDA content of tomato plants treated with NaCl, NaCl+PDA, NaCl+DA, NaCl+Zn/DA, NaCl+EZD and NaCl+ODBAC/SL-EZD after 20 treatment cycles ($n = 3$ independent experiments, bars represent the mean ± SD). Different letters indicate statistically significant differences based on one-way ANOVA and Tukey's HSD test analysis, $P < 0.05$.

the efflux of excess Na⁺. Simultaneously, it enhances *NHX1*-mediated Na⁺ transport into vacuoles, reducing Na⁺ toxicity in the cytoplasm and achieving ion compartmentalization. Additionally, dopamine restricts Na⁺ transport to leaves through *HKT1;2*, protecting photosynthetic tissues and indirectly maintaining a high K⁺/Na⁺ ratio, thereby enhancing plant salt tolerance. Compared with DA, ODBAC/SL-EZD markedly improved the utilization rate and potency of dopamine, enabling

plants to maintain beneficial K⁺/Na⁺ ratios amidst salinity stress. This development positions ODBAC/SL-EZD as an advanced strategy for fortifying plant resilience to salinity, which potentially increases agricultural yields in salt-afflicted terrains.

This study was intended to address the challenges of using dopamine to alleviate plant salt stress, which is difficult due to its tendency to self-polymerize and undergo adsorption by soil. A
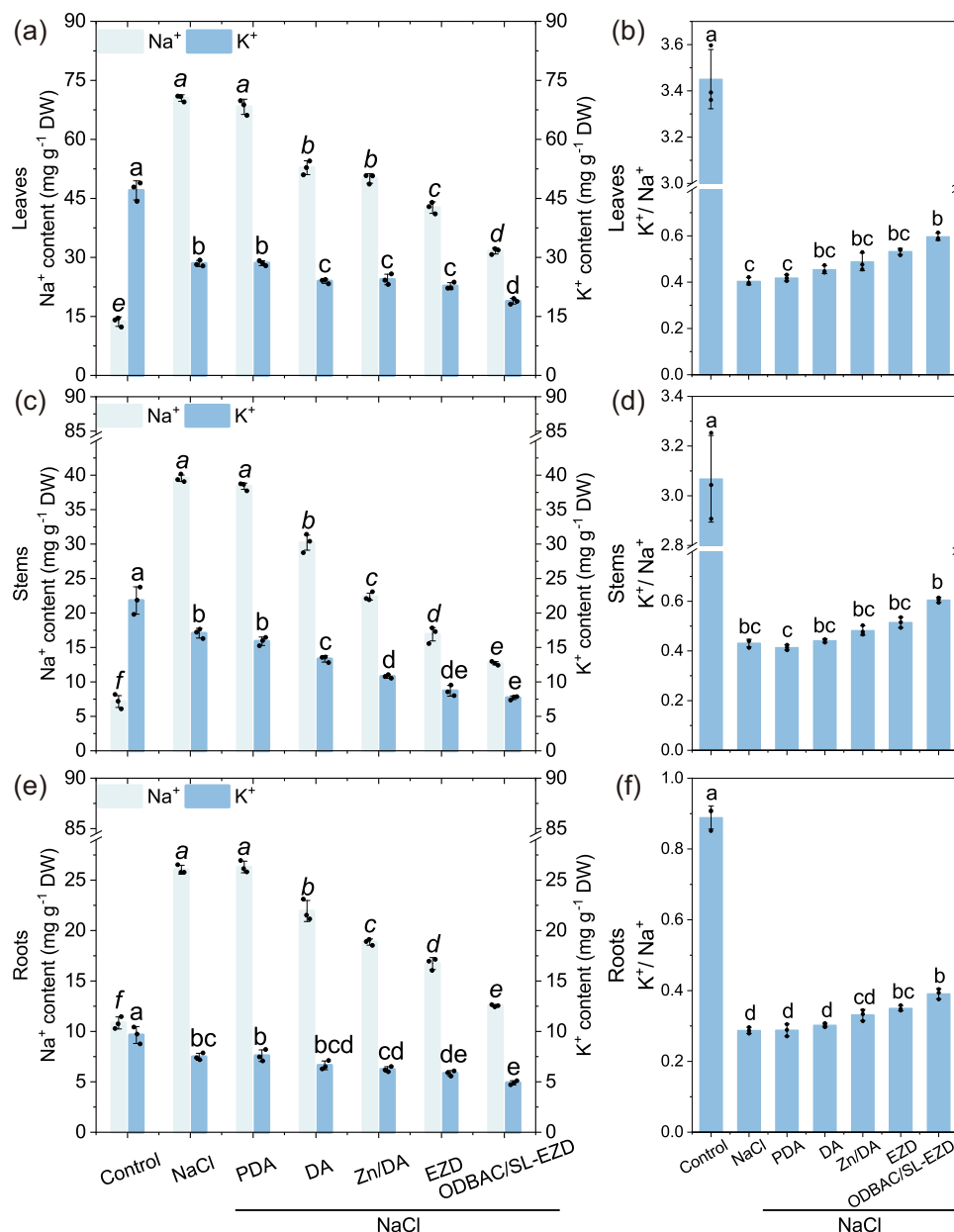
Fig. 7 | Effects of dopamine and its derivatives on distribution of K⁺ and Na⁺ in the leaves, stems and roots of tomato seedlings. The concentrations of Na⁺ and K⁺ in the (**a**) leaves, (**c**) stems, and (**e**) roots of tomato plants after 20 treatment cycles and the K⁺/Na⁺ ratios in the (**b**) leaves, (**d**) stems and (**f**) roots ($n = 3$ independent experiments, bars represent the mean ± SD. Different letters indicate statistically significant differences based on one-way ANOVA and Tukey's HSD test analysis, $P < 0.05$).

strategy was constructed in which a dual-ligand dopamine (EZD) was carried by a lignin-based nanoparticle (ODBAC/SL) via chelation and electrostatic attraction. This strategy significantly inhibited dopamine self-polymerization and its adsorption by soil. The ability of dopamine to alleviate plant salt stress was observed in both herbaceous and woody plants by increasing the K⁺/Na⁺ ratios, proline content, and antioxidant capacity. Nanotechnology significantly enhanced the efficacy of dopamine by mitigating soil absorption and facilitating uptake into plant roots. Overall, this modified strategy for dopamine significantly increased its application potential and provides an approach for alleviating plant salt stress.

Methods
Materials
Polyoxyethylene styrylphenyl ether was purchased from Zibo Yunchuan Chemicals Co., Ltd. (Shandong, China). EDTA, ODBAC, DA,

ZnSO₄•7H₂O, FeCl₃•6H₂O, FeSO₄•7H₂O, NaOH, dichloromethane and fluorescein isothiocyanate (FITC) were purchased from Aladdin Industrial Corporation (Shanghai, China). SL (molecular weights: 1.0×10^4–1.2×10^4) was purchased from MeadWestvaco Inc. (Virginia, USA).

Plant Material
Cultivation of *Solanum lycopersicum* cv 'Kaideyali 1832' and *Pyrus betulaefolia Bunge* No.1 seedlings were performed in a growth medium composed of a 3:1 volume ratio of peat to vermiculite. A climate-controlled growth chamber was utilized to ensure optimal growing conditions, featuring a light intensity of 250 µmol m⁻² s⁻¹, a 16/8-h day/night photoperiod, and temperatures regulated at 26 ± 2 °C (day) and 20 ± 2 °C (night), coupled with 60% relative humidity. The onset of salt stress treatments commenced once the tomato and pear seedlings reached 35 and 90 days old, respectively.
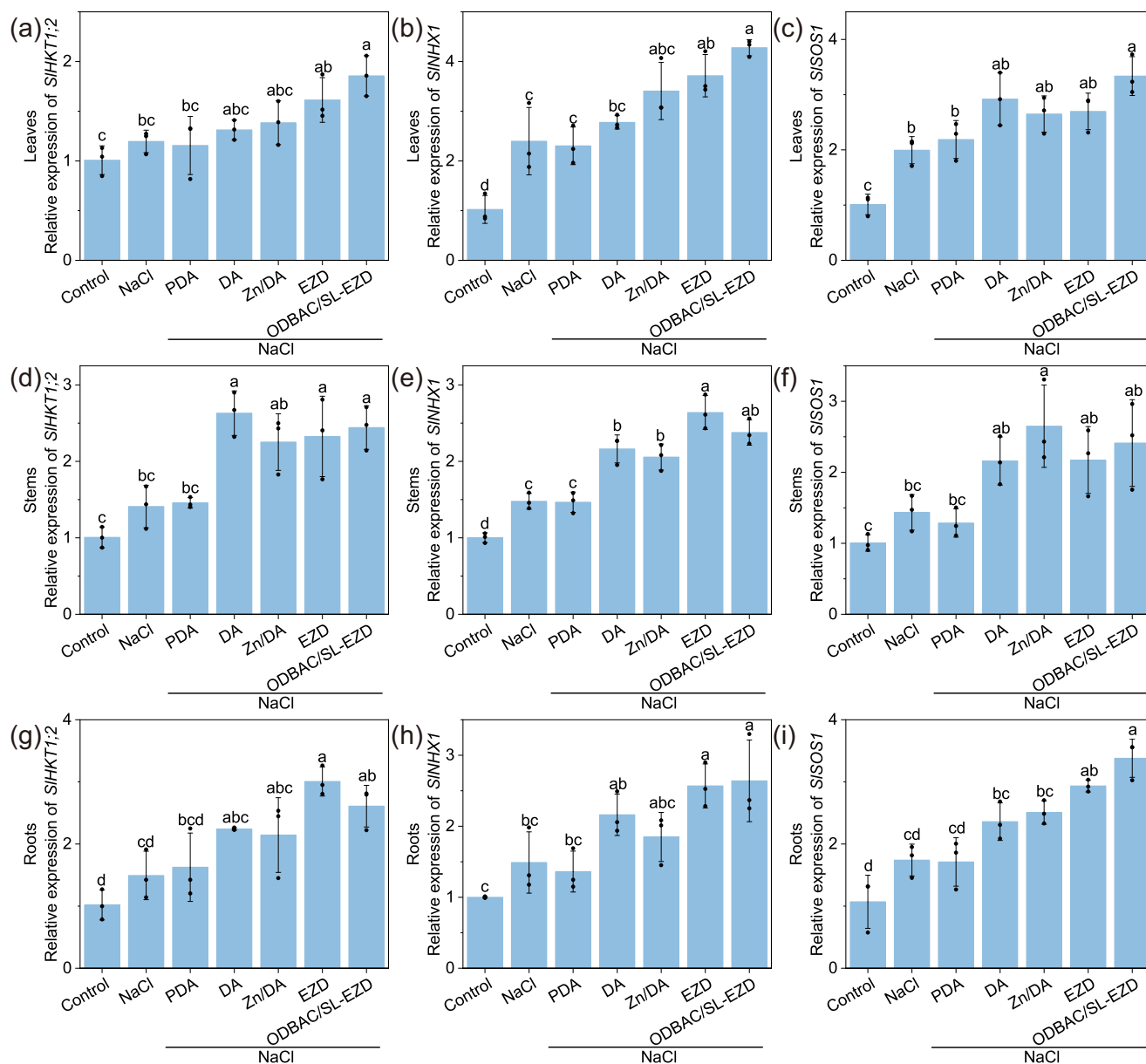
Fig. 8 | Effects of dopamine and its derivatives on the expression of Na$^+$ and K$^+$ transport-related genes in the leaves, stems and roots of tomato seedlings. Relative expression of *SlHKT1;2*, *SlNHX1* and *SlSOS1* in (**a**–**c**) leaves, (**d**–**f**) stems, and (**g**–**i**) roots of tomato plants after 20 treatment cycles (*n* = 3 independent experiments, bars represent the mean ± SD. Different letters indicate statistically significant differences based on one-way ANOVA and Tukey's HSD test analysis, *P* < 0.05).

Preparation of M/DA

ZnSO$_4$•7H$_2$O (0.080 g), FeSO$_4$•7H$_2$O (0.075 g), FeCl$_3$•6H$_2$O (0.0825 g), and DA (0.155 g) were dissolved in 10 mL deionized water, respectively. Then, the deionized water solution of metal ion (M) and the deionized water solution of DA were mixed under magnetic stirring at 400 rpm.

Preparation of EDTA/Zn

EDTA (0.335 g) and ZnSO$_4$ (0.080, 0.096, 0.112, 0.128, 0.144 or 0.160 g) were separately weighed and dissolved in 10 mL of deionized water, respectively. Subsequently, the deionized water solutions of EDTA and ZnSO$_4$ were mixed under magnetic stirring at a speed of 400 rpm to obtain different reaction ratios of EDTA/Zn.

Preparation of EZD

EDTA (0.335 g) and ZnSO$_4$•7H$_2$O (0.08 g or 0.128 g) were dissolved in 10 mL of deionized water, separately. The solutions of EDTA and ZnSO$_4$•7H$_2$O were then mixed under magnetic stirring at 400 rpm, and the pH value was adjusted to about 4 with NaOH. Subsequently, various quantities of DA were weighed and dissolved in 10 mL of deionized water. Considering that the theoretical reaction ratio of chelation between Zn and DA was 1:2, the ratio design of EZD was based on Zn: DA = 1:2 and was gradually decreased to 1:1.5, 1:1, and 1:0.5. The mixtures of EZD were prepared by mixing the above solutions, under magnetic stirring at 400 rpm, in the molar ratios of EDTA: Zn: DA = 1:0.5:1, 1:0.5:0.75, 1:0.5:0.5, 1:0.5:0.25, 1:0.8:1.6, 1:0.8:1.2, 1:0.8:0.8, and 1:0.8:0.4.

Preparation of ODBAC/SL and ODBAC/SL-EZD

ODBAC (0.50 g) and polyoxyethylene styrylphenyl ether (2.00 g) were dissolved in dichloromethane (5 mL) to form an oil phase. Then, 20 mL of deionized water was added to the oil phase to form an oil-in-water emulsion under stirring. Under stirring, SL (0.50 g) was dissolved in

50 mL deionized water. The ODBAC/SL was formed by mixing the oil-in-water emulsion and the SL aqueous solution. ODBAC/SL-EZD was obtained by mixing 10 mL ODBAC/SL solution with 10 mL EZD solution and stirring at 400 rpm for 8 h. FITC-ODBAC/SL and FITC-ODBAC/SL-EZD were synthesized by incorporating additional FITC into the oil phase and repeating the aforementioned procedures.

Self-polymerization of dopamine in tap water

DA, Zn/DA, and EZD (1:0.5:1, 1:0.5:0.75, 1:0.5:0.5, 1:0.5:0.25, 1:0.8:1.6, 1:0.8:1.2, 1:0.8:0.8, 1:0.8:0.4) samples were diluted with tap water to a dopamine concentration of 50 µmol L^{-1}. Subsequently, the samples were left at room temperature and their appearance was observed at 6, 48, and 96 h.

Characterization of EZD

UV-Vis spectrophotometer (UV-2600, Shimadzu, Japan) was used to detect the absorption value of DA in deionized dilution samples of DA, EDTA, EDTA/Zn, and EZD. The EZD powder obtained through vacuum freeze-dried was utilized for crystal structure analysis using XRD (Rigaku MiniFlex600, Japan). FTIR (Tensor II, Bruker Optics, Germany) was used to record the infrared spectrum of material.

Characterization of nanoparticles

The size distribution and *Zeta* potential of ODBAC/SL and ODBAC/SL-EZD were documented using a Zetasizer Nano ZS (NanoBrook, 90Plus PALS, Brookhaven, America). The nanoparticles underwent a cleaning process followed by subsequent testing. The morphology was observed using TEM (JEM-1400Plus, JEOL, Japan). The surface elemental composition of the nanoparticles was analyzed using XPS (ThermoFischer ESCALAB 250Xi, America). The thermal stability of the nanoparticles was evaluated using a thermogravimetric analyzer (TGA 55, Waters Corporation, America). Infrared spectra were recorded using FTIR, while crystal structure was examined through XRD analysis.

DA loading rate of ODBAC/SL

DA solutions with concentrations of 0.02 mg mL^{-1}, 0.04 mg mL^{-1}, 0.08 mg mL^{-1}, 0.12 mg mL^{-1}, and 0.14 mg mL^{-1} were prepared. Each solution was mixed with 0.8 mL of FeCl$_3$ (2.0×10^{-2} mol L^{-1}) and 0.5 mL of NH$_3 \cdot$H$_2$O, and then deionized water was added to give a total volume of 25 mL. This resulted in the formation of a purple–red complex. The absorbance of the purple–red complex at 507 nm was measured with a UV–Vis spectrophotometer. The linear relationship between the concentration of dopamine and the absorbance of the purple–red complex was evaluated, and the linear regression equation was calculated. The linear regression equation relating the concentration of DA and the absorbance of the purple–red complex was Y = 0.0067x−0.0438, R^2 = 0.9888.

The ODBAC/SL-EZD formulation (2 mL) was centrifuged at 16117 × g for 5 min, followed by placing the centrifuged nanoparticles in an oven at 60 °C for 24 h. The dried nanoparticles were mixed with 0.8 mL of an FeCl$_3$ (2.0×10^{-2} mol L^{-1}) solution and 0.5 mL of an NH$_3 \cdot$H$_2$O solution, and deionized water was added to give a constant volume of 25 mL. The absorbance of the purple–red complex at 507 nm was measured with a UV–Vis spectrophotometer. The load of DA was calculated with the following formula:

$$\text{Loading rate (\%)} = A/B \times 100 \tag{1}$$

where A is the weight of DA contained in the nanoparticles after drying and B is the weight of the nanoparticles after drying.

Adsorption of dopamine in soil

DA, Zn/DA, EZD = 1:0.5:0.5, EZD = 1:0.8:0.8 and ODBAC/SL-EZD were diluted with deionized water to a concentration of DA at 4 mmol L^{-1}.

Then, 20 mL of the diluent was added to sieved soil sample (5.00 g, 60-mesh). Vortex the mixture at 2800 rpm for 15 min, followed by centrifugation at 1791 × g for 5 min. Extract 5 mL of the supernatant and filter it using a 0.22 µm organic membrane filter. The ultraviolet spectra of 4 mmol L^{-1} DA standard solution and five groups of treated samples were detected by UV–Vis spectrophotometer.

Plant treatments

The tomato seedlings received daily irrigation with a variety of solutions across 7 different treatment regimens, including deionized water, 100 mmol L^{-1} NaCl solution, and solutions supplemented with 50 µmol L^{-1} concentrations (c(DA)) of PDA, DA, Zn/DA, EZD, or ODBAC/SL-EZD in the presence of 100 mmol L^{-1} NaCl. In contrast, the pear seedlings were subjected to bidaily treatments with analogous solutions, albeit at 150 mmol L^{-1} NaCl. Meanwhile, the alleviative effect of EZ and ODBAC/SL (in accordance with EZ and ODBAC/SL concentrations in ODBAC/SL-EZD) on salt stress was verified in line with the aforementioned method. Each treatment group included five biological replicates, with each replicate encompassing five individual plants.

Uptakes of FITC-ODBAC/SL-EZD in tomato roots

The FITC-ODBAC/SL-EZD was diluted to the dopamine concentration of 150 mmol L^{-1}, and tomato seedling roots were immersed in the dilution for 7 d. Subsequently, the roots were directly frozen sectioned, and the distribution of nanoparticles in the roots was observed by laser scanning confocal microscope (LSCM, LSM880, Zeiss, Germany).

Phenotypic assessment of plants subjected to salt stress

Alterations in growth, specifically seedling heights, were quantified using the Equation

$$H = H_N - H_{N-1} \tag{2}$$

where H_N is the height of the plants at the N survey post-treatment and H_{N-1} is the height of the plants at the N-1 survey post-treatment. The plant height was investigated once every 4 treatment cycles. Root morphology parameters (root lengths, number of root tips and root surface areas) were evaluated via high-resolution imaging of the root systems with a Scan Makeri800 Plus scanner (Shanghai Zhongjing Technology Co., Ltd., Shanghai, China), followed by the use of LA-S image analyser software (Hangzhou Wseen Testing Technology Co., Ltd., Hangzhou, China)[57]. To visually represent the typical treatment effects, a characteristic phenotype image from a single representative plant per treatment was captured.

Determination of chlorophyll content

After completing the tomato plant treatments, 0.2 g of the third fresh leaf from the top was collected and ground with a small amount of 90% ethanol solution. Once the tissue turned white during grinding, the volume was adjusted to 30 mL with 90% ethanol solution. The mixture was then shaken in the dark at room temperature for 15 min. Following centrifugation at 2579 × g for 30 s, absorbance was measured at 470 nm, 649 nm, and 665 nm using an ultraviolet spectrophotometer (V-1500, MACYLAB Instrument Co., Ltd., Shanghai, China). Chlorophyll content was calculated according to the method described by Yu et al.[58].

Determination of proline content

After 20 treatment cycles, 0.5 g of fresh leaves from the tomato plant were collected separately. The samples were thoroughly rinsed, placed in a mortar, and ground with 5 mL of sulfosalicylic acid. The resulting homogenate was collected and subjected to a 10-min boiling water bath. After cooling, the mixture was filtered to obtain the filtrate. For

each sample, 2 mL of the filtrate (or 2 mL of distilled water for the control) was taken, to which 2 mL of glacial acetic acid and 3 mL of acidic ninhydrin chromogenic solution were added. The mixture was heated in a boiling water bath for 40 min, then cooled to room temperature. Subsequently, 5 mL of toluene was added, and the solution was vigorously shaken and allowed to settle for phase separation. The upper toluene layer was carefully extracted and analyzed for absorbance at 520 nm using a spectrophotometer (V-1500, MACYLAB Instrument Co., Ltd., Shanghai, China), following the method described by Chen et al.[59].

Determination of O_2^- and MDA content

After 20 treatment cycles, individually collect 0.2 g of fresh leaves from the tomato plant. After thoroughly rinsing the samples, add 1 mL of phosphate buffer (0.05 mol L^{-1}, pH 7.8) to a mortar and grind the tissue on ice. Following grinding, rinse the mortar with an additional 3 mL of the buffer and collect the resulting extract. Centrifuge the extract at $10315 \times g$ for 20 min at 0–4 °C using a Herexi centrifuge (TG16MW, Herexi Instrument & Equipment Co., Ltd, Hunan, China) to obtain the supernatant. O_2^- activity was determined following the protocol of Elstner and Heupel[60], and MDA content was quantified using the thiobarbituric acid (TBA) method according to Gao et al.[10].

Quantification of Na$^+$ and K$^+$ concentrations

After 20 treatment cycles, seedlings exhibiting significant salt stress phenotypes were selected for ionic analysis. The plants were thoroughly rinsed with deionized water, followed by drying at 60 °C for 24 h. The desiccated specimens were then pulverized in a cryogenic environment using liquid nitrogen. For ionic content determinations, three 0.2 g aliquots each from the ground tissue were digested in a 20 mL mixture of 68% nitric acid and 30% hydrogen peroxide at a 2:1 volume ratio. The resulting solutions were assayed for Na$^+$ and K$^+$ concentrations using a flame photometer (Shanghai Jingke Industrial Co., Ltd., model FP640, Shanghai, China)[61].

RT-qPCR

Total RNA was extracted from the leaves, stems, and roots of tomato seedlings following the protocol provided with the FastPure Complex Tissue/Cell Total RNA Isolation Kit (Vazyme Biotech Co., Ltd., Nanjing, China). Complementary DNA (cDNA) was synthesized through reverse transcription using the PerfectStart® Green qPCR SuperMix (TransGen Biotech Co., Ltd., Beijing, China). Quantitative reverse transcription PCR (RT-qPCR) was performed using SlActin (NM_001308447.1) as the internal reference on the iCycler iQ5 system (Bio-Rad Laboratories, CA, USA). Relative gene expression levels were calculated using the $2^{-\Delta\Delta Ct}$ method (Liu et al.)[62]. All primers used for RT-qPCR were synthesized by Tsingke Biotech Co., Ltd. (Beijing, China), with primer sequences listed in Supplementary Table 1.

Data analysis

The data were statistically analyzed using Tukey's HSD test ($P < 0.05$) in *SPSS* software (version 22.0.) and are presented as the mean and standard deviations (SD). The data fitting and figure generation were performed using OriginPro 2018 software.

Reporting summary

Further information on research design is available in the Nature Portfolio Reporting Summary linked to this article.

Data availability

Source data is available for Figs. 2–4, 6–8 and Supplementary Figs. 5, 7, 10–12, 14, 15, 17–19 in the associated source data file. Source data are provided with this paper.

References

1. van Zelm, E. et al. Salt tolerance mechanisms of plants. *Annu. Rev. Plant Biol.* **71**, 403–433 (2020).
2. Munns, R. et al. Mechanisms of salinity tolerance. *Annu. Rev. Plant Biol.* **59**, 651–681 (2008).
3. Yu, Z. P. et al. How plant hormones mediate salt stress responses. *Trends Plant Sci.* **25**, 1117–1130 (2020).
4. Mickelbart, M. V. et al. Genetic mechanisms of abiotic stress tolerance that translate to crop yield stability. *Nat. Rev. Genet.* **16**, 237–251 (2015).
5. Ondrasek, G. et al. Salt stress in plants and mitigation approaches. *Plants-Basel* **11**, 717 (2022).
6. Zhu, T. et al. Ethylene and hydrogen peroxide are involved in brassinosteroid-induced salt tolerance in tomato. *Sci. Rep.* **6**, 35392 (2016).
7. Ha, C. V. et al. Positive regulatory role of strigolactone in plant responses to drought and salt stress. *Proc. Natl. Acad. Sci. USA* **111**, 851–856 (2014).
8. Lan, G. P. et al. Effects of dopamine on antioxidation, mineral nutrients, and fruit quality in cucumber under nitrate stress. *J. Plant Growth Regul.* **41**, 2918–2929 (2022).
9. Lan, G. P. et al. Effects of dopamine on growth, carbon metabolism, and nitrogen metabolism in cucumber under nitrate stress. *Sci. Hortic-Amsterdam.* **260**, 108790 (2020).
10. Gao, T. T. et al. Dopamine and arbuscular mycorrhizal fungi act synergistically to promote apple growth under salt stress. *Environ. Exp. Bot.* **178**, 104159 (2020).
11. Li, C. et al. Dopamine alleviates salt-induced stress in *Malus hupehensis*. *Physiol. Plant.* **153**, 584–602 (2014).
12. Yildirim, E. et al. Exogenous dopamine mitigates the effects of salinity stress in tomato seedlings by alleviating the oxidative stress and regulating phytohormones. *Acta Physiol. Plant.* **46**, 59 (2024).
13. Kang, X. M. et al. Revealing the formation mechanism of insoluble polydopamine by using a simplified model system. *Polym. Chem-Uk.* **8**, 860–864 (2017).
14. Yang, S. J. et al. Codeposition of levodopa and polyethyleneimine: reaction mechanism and coating construction. *Acs Appl. Mater. Inter.* **12**, 54094–54103 (2020).
15. Liang, B. et al. Dopamine alleviates nutrient deficiency-induced stress in *Malus hupehensis*. *Plant Physiol. Bioch.* **119**, 346–359 (2017).
16. Jia, X. et al. Adhesive polydopamine coated avermectin microcapsules for prolonging foliar pesticide retention. *Acs Appl. Mater. Inter.* **6**, 19552–19558 (2014).
17. Ji, Y. Z. et al. Adhesive nanocomposite for prolonging foliar retention and synergistic weeding and nourishing. *Adv. Sustain. Syst.* **4**, 2000010 (2020).
18. Ponzio, F. et al. Oxidant control of polydopamine surface chemistry in acids: a mechanism-based entry to superhydrophilic-superoleophobic coatings. *Chem. Mater.* **28**, 4697–4705 (2016).
19. Delparastan, P. et al. Direct evidence for the polymeric nature of polydopamine. *Angew. Chem. Int. Edit.* **58**, 1077–1082 (2018).
20. Lee, H. et al. Mussel-inspired surface chemistry for multifunctional coatings. *Science* **318**, 426–430 (2007).
21. Dreyer, D. R. et al. Elucidating the structure of poly(dopamine). *Langmuir* **28**, 6428–6435 (2012).
22. Khan, M. N. et al. Seed nanopriming: how do nanomaterials improve seed tolerance to salinity and drought? *Chemosphere* **310**, 136911 (2023).
23. Zhao, L. et al. Nano-biotechnology in agriculture: use of nanomaterials to promote plant growth and stress tolerance. *J. Agric. Food Chem.* **68**, 1935–1947 (2020).
24. Du, J. et al. One-pot construction of epoxy resin nanocarrier delivering abamectin and its efficacy on plant root-knot nematodes. *Pest. Manag. Sci.* **79**, 3103–3113 (2023).

25. Luo, J. et al. Pyraclostrobin loaded lignin-modified nanocapsules: delivery efficiency enhancement in soil improved control efficacy on tomato Fusarium crown and root rot. *Chem. Eng. J.* **394**, 124854 (2020).

26. Zhang, D. X. et al. Lignin-modified electronegative epoxy resin nanocarriers effectively deliver pesticides against plant root-knot nematodes (*Meloidogyne incognita*). *J. Agric. Food Chem.* **68**, 13562–13572 (2020).

27. Chen, L. et al. CeO_2 nanoparticles improved cucumber salt tolerance is associated with its induced early stimulation on antioxidant system. *Chemosphere* **299**, 134474 (2022).

28. El-Badri, A. M. et al. Mitigation of the salinity stress in rapeseed (*Brassica napus* L.) productivity by exogenous applications of bio-selenium nanoparticles during the early seedling stage. *Environ. Pollut.* **310**, 119815 (2022).

29. Moradbeygi, H. et al. Investigating the enzymatic and non-enzymatic antioxidant defense by applying iron oxide nanoparticles in *Dracocephalum moldavica* L. plant under salinity stress. *Sci. Hortic-Amsterdam.* **272**, 109537 (2020).

30. Ye, Y. Q. et al. Manganese nanoparticles control salinity-modulated molecular responses in *Capsicum annuum* L. through priming: a sustainable approach for agriculture. *Acs Sustain. Chem. Eng.* **8**, 1427–1436 (2020).

31. El-Badri, A. M. et al. Selenium and zinc oxide nanoparticles modulate the molecular and morpho-physiological processes during seed germination of *Brassica napus* under salt stress. *Ecotox. Environ. Safe.* **225**, 112695 (2021).

32. Avestan, S. et al. Application of nano-silicon dioxide improves salt stress tolerance in strawberry plants. *Agronomy-Basel* **9**, 246 (2019).

33. Kteeba, S. M. et al. Exposure to ZnO nanoparticles alters neuronal and vascular development in zebrafish: acute and transgenerational effects mitigated with dissolved organic matter. *Environ. Pollut.* **242**, 433–448 (2018).

34. Chen, T. H. et al. Zinc oxide nanoparticles alter hatching and larval locomotor activity in zebrafish (*Danio rerio*). *J. Hazard. Mater.* **277**, 134–140 (2014).

35. Zhao, Y. et al. Neurotoxicity of nanoparticles: insight from studies in zebrafish. *Ecotox. Environ. Safe.* **242**, 113896 (2022).

36. Dabour, K. et al. Cellular alterations in midgut cells of honey bee workers (*Apis millefera* L.) exposed to sublethal concentrations of CdO or PbO nanoparticles or their binary mixture. *Sci. Total Environ.* **651**, 1356–1367 (2019).

37. Tang, Q. Q. et al. Formation of uniform colloidal spheres based on lignosulfonate, a renewable biomass resource recovered from pulping spent liquor. *Acs Sustain. Chem. Eng.* **6**, 1379–1386 (2017).

38. Zhang, D. X. et al. Core/shell dual-responsive nanocarriers via iron-mineralized electrostatic self-assembly for precise pesticide delivery. *Adv. Funct. Mater.* **31**, 2102027 (2021).

39. Liu, Q. et al. A lignin-derived material improves plant nutrient bioavailability and growth through its metal chelating capacity. *Nat. Commun.* **14**, 4866 (2023).

40. Zhao, Q. et al. A metal chelator as a plasmonic signal-generation superregulator for ultrasensitive colorimetric bioassays of disease biomarkers. *Adv. Sci.* **5**, 1800295 (2018).

41. Chariou, P. L. et al. Soil mobility of synthetic and virus-based model nanopesticides. *Nat. Nanotechnol.* **14**, 712–718 (2019).

42. Chariou, P. L. et al. Delivery of pesticides to plant parasitic nematodes using tobacco mild green mosaic virus as a nanocarrier. *Acs Nano* **11**, 4719–4730 (2017).

43. Peng, R. F. et al. Preparation of self-dispersed lignin-based drug-loaded material and its application in avermectin nano-formulation. *Int. J. Biol. Macromol.* **151**, 421–427 (2020).

44. Shi, X. et al. A smart patch with on-demand detachable adhesion for bioelectronics. *Small* **17**, e2101220 (2021).

45. Ratinac, K. R. et al. Lignosulfonate adsorption on and stabilization of lead zirconate titanate in aqueous suspension. *J. Colloid Interf. Sci.* **273**, 442–454 (2004).

46. Yan, M. F. et al. Influence of pH on the behavior of lignosulfonate macromolecules in aqueous solution. *Colloid. Surface A.* **371**, 50–58 (2010).

47. Pan, S. H. et al. Preparation of enzyme-responsive composite nanocapsules with sodium carboxymethyl cellulose to improve the control effect of root-knot nematode disease. *Int. J. Biol. Macromol.* **241**, 124561 (2023).

48. Zhao, N. et al. Enzyme-responsive lignin nanocarriers for triggered delivery of abamectin to control plant root-knot nematodes (*Meloidogyne incognita*). *J. Agric. Food Chem.* **71**, 3790–3799 (2023).

49. Yang, Y. Q. et al. Unraveling salt stress signaling in plants. *J. Integr. Plant Biol.* **60**, 796–804 (2018).

50. Assaha, D. V. M. et al. The role of Na^+ and K^+ transporters in salt stress adaptation in glycophytes. *Front. Physiol.* **8**, 509 (2017).

51. Lin, H. X. et al. Phosphorylation of SOS3-LIKE CALCIUM BINDING PROTEIN8 by SOS2 protein kinase stabilizes their protein complex and regulates salt tolerance in *Arabidopsis*. *Plant Cell* **21**, 1607–1619 (2009).

52. Ren, Z. H. et al. A rice quantitative trait locus for salt tolerance encodes a sodium transporter. *Nat. Genet.* **37**, 1141–1146 (2005).

53. Rus, A. et al. AtHKT1 is a salt tolerance determinant that controls Na^+ entry into plant roots. *Proc. Natl. Acad. Sci. USA* **98**, 14150–14155 (2001).

54. Rus, A. et al. AtHKT1 facilitates Na^+ homeostasis and K^+ nutrition in planta. *Plant. Physiol.* **136**, 2500–2511 (2004).

55. Apse, M. P. et al. Vacuolar cation/H^+ exchange, ion homeostasis, and leaf development are altered in a T-DNA insertional mutant of AtNHX1, the *Arabidopsis vacuolar* Na^+/H^+ antiporter. *Plant J.* **36**, 229–239 (2003).

56. Blumwald, E. et al. Sodium transport in plant cells. *Bba-Biomembranes* **1465**, 140–151 (2000).

57. Li, H. et al. H_2S pretreatment mitigates the alkaline salt stress on *Malus hupehensis* roots by regulating Na^+/K^+ homeostasis and oxidative stress. *Plant Physiol. Bioch.* **156**, 233–241 (2020).

58. Yu, Y. A. et al. A wheat WRKY transcription factor *TaWRKY17* enhances tolerance to salt stress in transgenic *Arabidopsis* and wheat plant. *Plant Mol. Biol.* **113**, 171–191 (2023).

59. Chen, K. et al. MdMYB46 could enhance salt and osmotic stress tolerance in apple by directly activating stress-responsive signals. *Plant Biotechnol. J.* **17**, 2341–2355 (2019).

60. Elstner, E. F. et al. Inhibition of nitrite formation from hydroxylammoniumchloride: a simple assay for superoxide dismutase. *Anal. Biochem.* **70**, 616–620 (1976).

61. Liang, B. W. et al. Effects of exogenous dopamine on the uptake, transport, and resorption of apple ionome under moderate drought. *Front. Plant Sci.* **9**, 755 (2018).

62. Liu, M. H. et al. S-nitrosylation of ACO homolog 4 improves ethylene synthesis and salt tolerance in tomato. *New Phytol.* **239**, 159–173 (2023).

Author contributions

S.F., D.Z., J.D. and H.X. designed the project and interpreted the data. J.D. and H.X. performed the experiments. All authors wrote and edited the manuscript.

Competing interests

The authors declare no competing interests.

Additional information